

RECYCLING AUGMENTED LAGRANGIAN PRECONDITIONER IN AN INCOMPRESSIBLE FLUID SOLVER*

MAXIM A. OLSHANSKII[†] AND ALEXANDER ZHILIAKOV[‡]

Abstract. The paper discusses a reuse of matrix factorization as a building block in the Augmented Lagrangian (AL) and modified AL preconditioners for a non-symmetric saddle point linear algebraic systems. The strategy is applied to solve two-dimensional incompressible fluid problems with efficiency rates independent of the Reynolds number. The solver is then tested to simulate a motion of surface fluids, an example of 2D flows motivated by an interest in lateral fluidity of inextensible viscous membranes. Numerical examples include the Kelvin–Helmholtz instability problem posed on the sphere and on the torus.

Key words. Augmented Lagrangian preconditioner, grad-div stabilization, surface fluids, fluidic membranes, trace finite element method, Kelvin–Helmholtz instability

1. Introduction. Augmented Lagrangian (AL) preconditioning is a potent technique that has been developed to solve some highly non-symmetric algebraic systems having a saddle point structure [2, 3, 5, 12, 15, 22, 23, 24, 33, 40, 51]. The need to treat such problems numerically emerges from the discretization of systems of PDEs describing the motion of incompressible viscous fluid with dominating inertia effects. Adopting the terminology of fluid mechanics, the AL approach augments the velocity subproblem of the system using a suitably weighted incompressibility constraint. This leads to a well conditioned pressure Schur complement matrix, but makes the velocity submatrix more difficult to solve or to precondition. Already in the original work [2] a special multigrid method has been used to overcome the difficulty associated with preconditioning the velocity block, and recently this technique was extended in [16, 17]. Nevertheless, the specialized multilevel approach is efficient only if a hierarchy of nested discretizations is available and only for certain finite element velocity–pressure pairs. In the present paper we advocate a more general, but still efficient, way to handle the velocity subproblem in the AL approach. The proposed method consists of computing (possibly incomplete) LU factorization of the velocity block (or velocity sub-blocks in a modified AL approach) with further recycling of the factors over several next time steps. The factorization can be updated when the velocity field variations significantly change the transport term in the equations. A simpler strategy adopted here consists of updating preconditioner when the number of FGMRES iterations exceeds a threshold. We shall see that for realistic unsteady 2D flows this results in a very efficient approach, which is robust with respect to the Reynolds number and calls for only a small number of full factorizations over a long-time simulation.

Employing matrix factorizations in algebraic solvers for equations governing the flow of viscous incompressible fluids is not a new theme. It is standard to factorize

*This work was partially supported by US National Science Foundation (NSF) through grants DMS-1953535 and DMS-2011444.

[†]Department of Mathematics, University of Houston, Houston, Texas 77204 (molshan@math.uh.edu)

[‡]Department of Mathematics, University of Houston, Houston, Texas 77204 (alex@math.uh.edu)

the discrete pressure Poisson equation. More recently, studies were done regarding different strategies to perform incomplete LU factorization of the coupled systems for velocity and pressure [11, 29, 30, 48]. We note that the latter cannot be done with the help of position-based ILU, since the pressure block in the matrix may be zero. The augmented Lagrangian approach provides a framework to apply factorization only to the velocity matrix, while retaining the overall excellent preconditioning properties. The velocity matrix results from the discretization of an elliptic part of the system. Therefore it is typically a positive definite matrix and LU factorization is stable without any preprocessing.

Large scale 3D simulations lead to algebraic systems which are still too expensive to factorize exactly and alternative ways of treating the velocity submatrix, e.g. based on geometric/algebraic multigrid, domain decomposition methods or incomplete factorization, can be more feasible and practical. The situation is different for 2D problems, where acceptable resolution is often achieved using the number of degrees of freedom affordable by state-of-the-art direct solvers executed on a desktop machine. Traditionally 2D flows have been considered as a mathematical idealization of real-life 3D phenomena. However, recently we see a surge of interest in understanding and solving fluid systems posed on 2D surfaces (see, e.g., [4, 6, 18, 20, 25, 27, 31, 34, 35, 41, 43, 44, 46]) as physically motivated continuum based models of thin material layers exhibiting lateral viscosity such as lipid bilayers and plasma membranes [21, 45, 49].

This recent interest in models describing lateral fluidity of material surfaces motivates our choice of the test fluid problem here. We consider the Navier–Stokes equations posed on a geometrically steady surface. These equations govern the tangential viscous motions of the surface fluid subject to the inextensibility condition. A geometrically unfitted discretization technique known as the trace finite element method (Trace FEM) [38, 42] is applied to handle the systems numerically. The augmentation is added on continuous level in the form of the grad-div stabilization [39, 37]. A preconditioned iterative method with recycled factorizations is then applied to solve the linearized Navier–Stokes equations on each time step of numerical simulations. The whole approach is used to compute two interesting surface flows: the Kelvin–Helmholtz instability problem on a sphere and a torus. We observe a notable difference in the evolution of (large) vortices in these two settings.

The remainder of the paper consists of three sections. In section 2 we recall the surface Navier–Stokes equations and apply \mathbf{P}_2 – P_1 Trace FEM to discretize them. Section 3 considers the properties of the resulting linear algebraic systems, introduces a preconditioner and recycling strategy. Finally, section 4 collects and discusses the results of numerical experiments.

2. Surface Navier–Stokes problem and its discretization. Consider a closed sufficiently smooth surface Γ embedded in \mathbb{R}^3 . For \mathbf{n} , the outward pointing unit normal on Γ , the orthogonal projection on the tangential plane is given by $\mathbf{P} = \mathbf{P}(\mathbf{x}) := \mathbf{I} - \mathbf{n}(\mathbf{x})\mathbf{n}(\mathbf{x})^T$, $\mathbf{x} \in \Gamma$. Following [25] we formulate the surface fluid equation in terms of tangential differential calculus. To this end, we assume smooth extensions of a scalar function $p : \Gamma \rightarrow \mathbb{R}$ or a vector function $\mathbf{u} : \Gamma \rightarrow \mathbb{R}^3$ to a neighborhood $\mathcal{O}(\Gamma)$ of Γ . For example, one can consider extension along the normal directions using the

closest point mapping $\mathbf{p} : \mathcal{O}(\Gamma) \rightarrow \Gamma$. The surface gradient and covariant derivatives on Γ are then defined as $\nabla_\Gamma p = \mathbf{P}\nabla p^e$ and $\nabla_\Gamma \mathbf{u} := \mathbf{P}\nabla \mathbf{u}^e \mathbf{P}$. The definitions of surface gradient and covariant derivatives are independent of a particular smooth extension of p and \mathbf{u} off Γ . The surface rate-of-strain tensor [21] is given by $E_s(\mathbf{u}) := \frac{1}{2}(\nabla_\Gamma \mathbf{u} + \nabla_\Gamma \mathbf{u}^T)$, and the surface divergence operators for a vector $\mathbf{u} : \Gamma \rightarrow \mathbb{R}^3$ and a tensor $\mathbf{A} : \Gamma \rightarrow \mathbb{R}^{3 \times 3}$ are defined as

$$\operatorname{div}_\Gamma \mathbf{u} := \operatorname{tr}(\nabla_\Gamma \mathbf{u}), \quad \operatorname{div}_\Gamma \mathbf{A} := (\operatorname{div}_\Gamma(\mathbf{e}_1^T \mathbf{A}), \operatorname{div}_\Gamma(\mathbf{e}_2^T \mathbf{A}), \operatorname{div}_\Gamma(\mathbf{e}_3^T \mathbf{A}))^T,$$

with \mathbf{e}_i the i th basis vector in \mathbb{R}^3 .

The conservation of momentum for a thin material layer together with the inextensibility condition and assumption of vanishing normal motions (geometric equilibrium) leads to the following surface Navier–Stokes problem: Given area forces $\mathbf{f} \in L^2(\Gamma)^3$, with $\mathbf{f} \cdot \mathbf{n} = 0$, find a vector field $\mathbf{u} : [0, T] \times \Gamma \rightarrow \mathbb{R}^3$, with $\mathbf{u}(0, \cdot) = \mathbf{u}_0$, $\mathbf{u} \cdot \mathbf{n} = 0$, and $p : [0, T] \times \Gamma \rightarrow \mathbb{R}$ such that

$$\begin{cases} \rho \left(\frac{\partial \mathbf{u}}{\partial t} + (\nabla_\Gamma \mathbf{u}) \mathbf{u} \right) - 2\nu \mathbf{P} \operatorname{div}_\Gamma(E_s(\mathbf{u})) + \nabla_\Gamma p = \mathbf{f} & \text{on } \Gamma, \\ \operatorname{div}_\Gamma \mathbf{u} = 0 & \text{on } \Gamma. \end{cases} \quad (2.1)$$

Here \mathbf{u} is the tangential fluid velocity, p is the surface fluid pressure, ρ and ν are density and viscosity coefficients. We further assume ν , p and \mathbf{f} re-scaled so that $\rho = 1$.

For the discretization of (2.1) we apply the trace \mathbf{P}_2 – P_1 FEM [43]. To apply the method, assume Γ is strictly contained in a polygonal domain $\Omega \subset \mathbb{R}^3$ and consider a family $\{\mathcal{T}_h\}_{h>0}$ of shape regular tetrahedral tessellations of Ω . The subset of tetrahedra that have a nonzero intersection with Γ is collected in the set denoted by \mathcal{T}_h^Γ with the characteristic mesh size h , and $\overline{\Omega}_h^\Gamma = \bigcup \{\overline{T} : T \in \mathcal{T}_h^\Gamma\}$. On $\overline{\Omega}_h^\Gamma$ we consider the standard H^1 -conforming finite element spaces of degree k ,

$$V_h^k = \{v \in C(\Omega_h^\Gamma) : v \in P_k(T) \text{ for any } T \in \mathcal{T}_h^\Gamma\}, \quad \text{with } k = 1, 2.$$

The velocity and pressure bulk finite element spaces are then defined to be

$$\mathbf{V}_h := (V_h^2)^3, \quad Q_h := V_h^1 \cap L_2^0(\Gamma).$$

The finite element formulation uses the restrictions (traces) of these spaces on Γ . Note that the traces of vector functions from \mathbf{V}_h does not necessarily satisfy the tangentiality $\mathbf{u} \cdot \mathbf{n} = 0$ condition. It is not straightforward, if possible at all, to build an H^1 -conforming finite element method which is also conformal with respect to the tangentiality condition. Therefore, the tangentiality condition will be enforced weakly by a penalty method. We shall also need an extension of the normal vector from Γ to Ω_h^Γ , which we define as $\mathbf{n} = \nabla d$, where d is the signed distance function to Γ . In practice, d is often not available and thus we use approximations. We introduce the

following finite element bilinear forms:

$$\begin{aligned}
a(\mathbf{u}, \mathbf{v}) &:= 2\nu \int_{\Gamma} E_s(\mathbf{u}) : E_s(\mathbf{v}) ds + \tau \int_{\Gamma} (\mathbf{n} \cdot \mathbf{u})(\mathbf{n} \cdot \mathbf{v}) ds + \rho_u \int_{\Omega_h^{\Gamma}} [(\mathbf{n} \cdot \nabla) \mathbf{u}] \cdot [(\mathbf{n} \cdot \nabla) \mathbf{v}] dx, \\
\gamma(\mathbf{u}, \mathbf{v}) &:= \widehat{\gamma} \int_{\Gamma} \operatorname{div}_{\Gamma} \mathbf{u} \operatorname{div}_{\Gamma} \mathbf{v} ds, \\
s(p, q) &:= \rho_p \int_{\Omega_h^{\Gamma}} (\mathbf{n} \cdot \nabla p)(\mathbf{n} \cdot \nabla q) dx.
\end{aligned}$$

The forms are well defined for $p, q \in H^1(\Omega_h^{\Gamma})$, $\mathbf{u}, \mathbf{v} \in H^1(\Omega_h^{\Gamma})^3$. Here $\tau > 0$ is a penalty parameter and $\rho_u \geq 0$, $\rho_p \geq 0$ are stabilization parameters, which we set according to [43]:

$$\tau = h^{-2}, \quad \rho_p = h, \quad \rho_u = 1. \quad (2.2)$$

Note that both stabilization terms vanish if \mathbf{u} and p is the surface solution extended along normal directions to a neighborhood of Γ . This makes the finite element formulation consistent. At the same time, both terms add to the finite element formulation additional ‘‘stiffness’’ in the normal direction. This allows to eliminate the dependence of the resulting algebraic systems conditioning on the position of Γ in the background mesh, the idea first suggested for trace FEM in [7] and later explored in many publications on unfitted FEM for surface PDEs, e.g. [8, 9, 19] (the particular choice of stabilization terms varies in the literature). We refer to [43] for the further discussion of the role of these terms in the context of unfitted \mathbf{P}_2 - P_1 elements and the proof of Γ -independent estimates on the condition numbers of the velocity and pressure matrix. The implementation of the bilinear form $\gamma(\mathbf{u}, \mathbf{v})$ uses the identity

$$\int_{\Gamma} \operatorname{div}_{\Gamma} \mathbf{u}_h \operatorname{div}_{\Gamma} \mathbf{v}_h ds = \int_{\Gamma} \operatorname{tr} E_s(\mathbf{u}_h) \operatorname{tr} E_s(\mathbf{v}_h) ds.$$

We shall comment on the role of this form below.

Assuming a constant time step $\Delta t = T/N$, the semi-implicit in time finite element discretization of (2.1) reads: Given $\mathbf{u}_h^{k-1}, \mathbf{u}_h^{k-2} \in \mathbf{V}_h$, find $(\mathbf{u}_h^k, p_h^k) \in \mathbf{V}_h \times Q_h$ solving

$$\begin{aligned}
([\mathbf{u}_h]_t^k, \mathbf{v}_h) + a(\mathbf{u}_h^k, \mathbf{v}_h) + c(\widetilde{\mathbf{u}}_h^k, \mathbf{u}_h^k, \mathbf{v}_h) + \gamma(u_h, v_h) + b(\mathbf{v}_h, p_h^k) &= (\mathbf{f}^k, \mathbf{v}_h) \\
b(\mathbf{u}_h^k, q_h) - s_h(p_h^k, q_h) &= 0
\end{aligned} \quad (2.3)$$

for all $\mathbf{v}_h \in \mathbf{V}_h$ and $q_h \in Q_h$, $k = 2, 3, \dots, N$. We used the notation $\mathbf{u}_h^k(\mathbf{x}) \simeq \mathbf{u}(t^k, \mathbf{x})$, $t^k = k\Delta t$ and similar for p_h^k . In numerical experiments we employ the second order method with

$$[\mathbf{u}_h]_t^k = \frac{3\mathbf{u}_h^k - 4\mathbf{u}_h^{k-1} + \mathbf{u}_h^{k-2}}{2\Delta t}, \quad \widetilde{\mathbf{u}}_h^k = 2\mathbf{u}_h^{k-1} - \mathbf{u}_h^{k-2}, \quad (2.4)$$

but this particular choice has little effect on the properties of the resulting linear systems. The fourth term in (2.3) is the surface analogue of the grad-div stabilization [39, 37]. We further set the grad-div stabilization parameter

$$\widehat{\gamma} = 1 \quad (2.5)$$

unless it is stated otherwise and write $\gamma = \hat{\gamma}$ to simplify the notation. It is interesting that no other stabilization was found to be necessary for computations with high Reynolds numbers. A possible explanation is that tangential flows do not produce boundary layers (on a closed surface) and, in addition, the grad-div term by itself is known to dissipate excessive energy in under-resolved simulation [36, 28].

We conclude this section noting that the implementation requires the integration of polynomial functions over Γ . In practice this is avoided by approximating Γ by some Γ_h which admits exact quadrature rules. The quantification of the introduced geometric inconsistency in the case of the Stokes problem and \mathbf{P}_k - P_{k-1} , $k = 2, 3, \dots$, trace elements is given in [26].

3. System of linear algebraic equations and preconditioning. We see that on each time step the linearized problem in (2.3) corresponds to the finite element discretization of the Oseen-type system

$$\begin{aligned} \alpha \mathbf{u} + \mathbf{P}(\mathbf{w} \cdot \nabla) \mathbf{u} - 2\nu \mathbf{P} \operatorname{div}_\Gamma(E_s(\mathbf{u})) + \nabla_\Gamma p &= \mathbf{f}, \\ \operatorname{div}_\Gamma \mathbf{u} &= 0 \end{aligned} \quad (3.1)$$

with $\alpha \simeq \Delta t^{-1}$ and the wind field \mathbf{w} . Hence the resulting systems of linear algebraic equations is non-symmetric and of saddle-point type with properties resembling those of the planar Oseen system, well-studied problem; see, e.g. [1, 14]. In particular, the problem is increasingly hard to solve when ν goes to zero.

A weak formulation of (3.1) needs the closed subspace of $H^1(\Gamma)^3$ consisting of *tangential* vector fields, $\mathbf{V}_T := \{\mathbf{v} \in H^1(\Gamma)^3 \mid \mathbf{v} \cdot \mathbf{n} = 0\}$. \mathbf{V}_T serves as the velocity trial and test space in a (velocity–pressure) weak formulation. For the penalty weak formulation one allows for the larger velocity space: $\{\mathbf{v} \in L^2(\Gamma)^3 : \mathbf{P}\mathbf{v} \in \mathbf{V}_T\}$. The well-posedness of both formulation relies on the surface Korn inequality (see (4.8) in [25]): There exists a constant $c_K > 0$ such that

$$\|\mathbf{u}\|_{L^2(\Gamma)} + \|E_s(\mathbf{u})\|_{L^2(\Gamma)} \geq c_K \|\mathbf{u}\|_{H^1(\Gamma)} \quad \text{for all } \mathbf{u} \in \mathbf{V}_T, \quad (3.2)$$

and the inf-sup condition (Lemma 4.2 in [25]): There exists a constant $c_0 > 0$ such that the following holds:

$$\inf_{p \in L_0^2(\Gamma)} \sup_{\mathbf{v} \in \mathbf{V}_T} \frac{\int_\Gamma q \operatorname{div}_\Gamma \mathbf{u} \, ds}{\|\mathbf{v}\|_{H^1(\Gamma)} \|p\|_{L^2(\Gamma)}} \geq c_0. \quad (3.3)$$

We now turn to the matrix form of the discretized Oseen system and define the velocity, pressure stabilization and divergence constraint matrices:

$$\begin{aligned} \mathbf{A}_{i,j} &= \alpha(\psi_j, \psi_i)_{L^2(\Gamma)} + a(\psi_j, \psi_i) + c(\mathbf{w}, \psi_j, \psi_i) + \gamma(\mathbf{u}_h, \mathbf{v}_h), \\ \mathbf{C}_{k,m} &= s(\xi_k, \xi_m) \quad \mathbf{B}_{k,i} = b(\psi_i, \xi_k), \end{aligned}$$

where $\{\psi_i\}$ and $\{\xi_k\}$ are the velocity and pressure nodal basis functions spanning \mathbf{V}_h and Q_h , respectively. After arranging velocity degrees of freedom first and pressure degrees of freedom next, we arrive at the system with the 2×2 -block matrix:

$$\underbrace{\begin{bmatrix} \mathbf{A} & \mathbf{B}^T \\ \mathbf{B} & -\mathbf{C} \end{bmatrix}}_{\mathcal{A}} \begin{bmatrix} \mathbf{u} \\ p \end{bmatrix} = \begin{bmatrix} \mathbf{f} \\ 0 \end{bmatrix}. \quad (3.4)$$

An important matrix related to the above system is the pressure Schur complement $\mathbf{S} = \mathbf{B}\mathbf{A}^{-1}\mathbf{B}^T + \mathbf{C}$, which results after elimination of the velocity unknowns from the system. A preconditioner for \mathbf{S} is a necessary ingredient for most iterative solvers that exploit the block structure of \mathcal{A} . Following a common practice [14] we consider the block-triangle right preconditioner for \mathcal{A} :

$$\mathcal{P} := \begin{pmatrix} \widehat{\mathbf{A}} & \mathbf{B}^T \\ & \widehat{\mathbf{S}} \end{pmatrix}, \quad (3.5)$$

where $\widehat{\mathbf{A}}$ and $\widehat{\mathbf{S}}$ are preconditioners for \mathbf{A} and \mathbf{S} , respectively.

For the next step, we define the surface pressure mass matrix \mathbf{M}_p and the pressure Laplace–Beltrami matrix \mathbf{L}_p :

$$(\mathbf{M}_p)_{k,m} = \int_{\Gamma} \xi_k \xi_m ds, \quad (\mathbf{L}_p)_{k,m} = \int_{\Gamma} \nabla_{\Gamma} \xi_k \cdot \nabla_{\Gamma} \xi_m ds.$$

For the surface Stokes problem ($\alpha = 0$, $\mathbf{w} = 0$, $\gamma = 0$, $\nu = 1$) matrix \mathbf{S} is spectrally equivalent to the stabilized pressure mass matrix $\mathbf{M}_p + \mathbf{C}$; see [43]. However, for $\mathbf{w} \neq 0$ and $\nu \rightarrow 0$ the problem of building a suitable preconditioner for \mathbf{S} is known to be particularly difficult. To circumvent it, the authors of [2] introduced an augmentation to the \mathbf{A} block of the system, which in the present paper is given by the grad-div term. In particular, for the planar Oseen problem discretized with \mathbf{P}_2 – P_1 elements one can show that the Schur complement of the augmented matrix is spectrally equivalent to the pressure mass matrix scaled by $(\gamma + \nu)^{-1}$ for sufficiently large γ [2]. We expect that similar property holds in the surface case and define the Schur complement preconditioner through its inverse as follows:

$$\widehat{\mathbf{S}}^{-1} := ((\nu + \gamma)^{-1} \mathbf{M}_p + \mathbf{C})^{-1} + (\alpha^{-1} \mathbf{L}_p + \mathbf{C})^{-1} \quad (3.6)$$

The second term is included to deal with the dominating reaction term in the Oseen problem (3.1) and the whole structure of $\widehat{\mathbf{S}}^{-1}$ resembles the Cahouet–Chabard preconditioner [10]. We apply several CG iterations to compute the action of $(\alpha^{-1} \mathbf{L}_p + \mathbf{C})^{-1}$ and $((\nu + \gamma)^{-1} \mathbf{M}_p + \mathbf{C})^{-1}$ on a vector.

As we discussed, the augmentation has the downside of adding to the (1,1)-block the term with a large nullspace. For larger γ this makes the matrix \mathbf{A} poor conditioned and hinders the efficiency of standard iterative methods to evaluate \mathbf{A}^{-1} . For certain finite elements (but not for the Taylor–Hood pairs) efficient geometric multi-grid method are known [16, 17] to deliver a preconditioner for \mathbf{A} robust with respect to the variation of parameters ν , γ , α . As a more flexible alternative we explore here the direct LU factorization of \mathbf{A} (or its sub-blocks) and the reuse of the factors for several time steps. In pursuing this line, we consider two strategies of building $\widehat{\mathbf{A}}$:

1. LU factorization of the full velocity block \mathbf{A} (full AL approach);
2. Velocity unknowns are enumerated componentwise so that \mathbf{A} attains the 3×3 -block form. Next $\widehat{\mathbf{A}}$ is obtained from \mathbf{A}_{tr} , the block upper-triangle part of \mathbf{A} , by applying LU factorization to each individual diagonal block of \mathbf{A}_{tr} . This corresponds to modified AL approach from [3].

The modified AL approach allows to handle smaller and better structured matrices that have the structure of a stiffness matrix of a conforming FEM applied to an elliptic scalar PDE. This enhanced efficiency comes with a price of slight ν and h dependence of the preconditioner performance [3]. We shall see below that in the case of time-dependent 2D flow the price is very tolerable.

Same approaches, of course, apply to reusing ILU factorizations, but we fix our idea and consider below exact LU. The surface fluid problem is essentially 2D and the number of velocity unknowns allows applying LU factorization. Furthermore, in a curvilinear metric the viscosity term does not simplify to Laplace operators for each velocity component, therefore adding the γ -term does not contribute to the sparsity pattern of the matrix (in contrast to the augmentation in the planar case). To make the algorithm precise, denote by $\mathbf{L}(k)$ and $\mathbf{U}(k)$ the LU factors of $\mathbf{A}(k)$ at step k of (2.3). We let $\hat{\mathbf{A}} = \mathbf{L}(k)\mathbf{U}(k)$ to be the preconditioner for all $\mathbf{A}(k+m)$, $m = 0, \dots, M$, where $M \geq 0$ is the largest index such that

$$\frac{\#\text{Iter}_{\text{FGMRES}}(k+m)}{\#\text{Iter}_{\text{FGMRES}}(k)} \leq \kappa, \quad \text{for } m = 0, \dots, M, \quad (3.7)$$

where $\kappa \geq 1$ is a maximum allowed increase of the preconditioned FGMRES iterations without updating the preconditioner.

4. Numerical simulations. We apply the trace FEM as described in section 2 to simulate the mixing layer of isothermal incompressible viscous surface fluid at several Reynolds numbers. The setup resembles the classical problem of the Kelvin–Helmholtz instability: For a detailed discussion of the planar analogue we refer to [47] and references therein. At higher Reynolds numbers the flow exhibits sharp internal layers and intensive vortical dynamics, offering a good test problem for both discretizations and flow solvers.

For discretization, an initial triangulation \mathcal{T}_{h_0} was build by dividing $\Omega = (-\frac{5}{3}, \frac{5}{3})^3$ into 2^3 cubes and further splitting each cube into 6 tetrahedra with $h_0 = \frac{5}{3}$. Further, the mesh is refined only close to the surface, and $\ell \in \mathbb{N}$ denotes the level of refinement so that $h_\ell = \frac{5}{3} 2^{-\ell}$. The trace \mathbf{P}_2 – P_1 Taylor–Hood finite element method with BDF2 time stepping is applied as described in (2.3)–(2.4), with the choice of parameters in (2.2) and (2.5). No further stabilizing terms, e.g., of streamline diffusion type, were included in the method, since the computed solutions do not reveal any spurious modes. We would like the discretization error, which results from the approximation of Γ , to be consistent with the higher order interpolation properties of \mathbf{P}_2 elements [26]. To address this, we apply additional refinement to define a piecewise-linear surface Γ_h used for the purpose of numerical integration as described in [43, section 6.3]. Software packages DROPS [13] and Belos, Amesos from Trilinos [50] were used for matrices assembling and algebraic solver execution, respectively. Because of the additional refinement used to define numerical quadratures, the matrix assembling time grows superlinear in our examples. The optimal complexity here can be obtained by using isoparametric higher order trace elements [32], not however implemented in the software we use.

4.1. The Kelvin–Helmholtz instability problem setup. There are very limited numerical studies of the Kelvin–Helmholtz (KH) problem for surface fluids.

Examples of an isothermal KH flows on cylinder and on the unit sphere are given in [31, 26]. Here we use the sphere example and for the first time simulate the KH flow on a torus of revolution.

The design of numerical experiment for the sphere follows [31, 26]. For $\Gamma = S^2$, let ξ and ζ to be renormalized azimuthal and polar coordinates, respectively: $-1/2 \leq \xi, \zeta < 1/2$. The tangent basis direction are $\mathbf{e}_\xi := \nabla_\Gamma \xi / \|\nabla_\Gamma \xi\|$ and $\mathbf{e}_\zeta := \nabla_\Gamma \zeta / \|\nabla_\Gamma \zeta\|$. The initial velocity field is given by the counter-rotating upper and lower hemispheres with velocity speed approximately equal 1 closer to equator and vanishing at poles. The velocity field has a sharp transition layer along equator, where we add perturbation to trigger the development of the vortical strip:

$$\begin{aligned} \mathbf{u}_0(\xi, \zeta) &:= d(\zeta)(\tanh(2\zeta/\delta_0)\mathbf{e}_\xi + c_n \mathbf{curl}_\Gamma \psi), \\ \psi(\xi, \zeta) &:= e^{-(\zeta/\delta_0)^2} (a_a \cos(m_a \pi \xi) + a_b \cos(m_b \pi \zeta)), \end{aligned} \quad (4.1)$$

where d is the distance from Γ to the z -axis. We take $\delta_0 := 0.05$ (for $|z| \gtrsim \delta_0$ the velocity field is close to a rigid body rotation around the z -axis), $c_n := 10^{-2}$ (perturbation parameter), and $a_a = 1$, $m_a = 16$, $a_b = 0.1$, $m_b = 20$ (perturbation magnitudes and frequencies). Note that \mathbf{u}_0 is tangential by construction, $\mathbf{u}_0 \cdot \mathbf{n} = 0$. The Reynolds number $\text{Re} \simeq \nu^{-1} \delta_0$ is based on $\|\mathbf{u}\|_{L^\infty(\Gamma)} \simeq 1$ and the initial layer width. We ran numerical simulations for $\nu = \frac{1}{2} 10^{-k}$, for $k = 3, 4, 5$, which corresponds to $\text{Re} = 10^k$, $k = 2, 3, 4$.

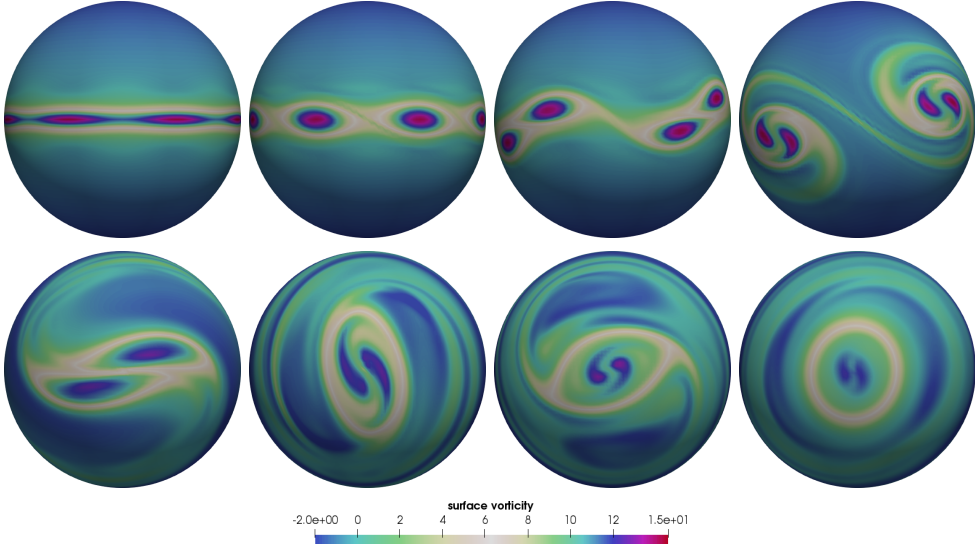


Fig. 4.1: KH flow at $\text{Re} = 10^4$. Snapshots of surface vorticity $w_h = \text{curl}_{\Gamma_h} \mathbf{u}_h$ for $t \in \{0, 2.5, 5, 6.25, 10, 12.5, 15, 20\}$. Click [here](#) for the full animation.

In Figure 4.1 we show several snapshots of the surface vorticity distributions starting from the initial condition. The solution reproduces the well known flow pattern of the planar KH instability development, which includes the initial vortices formation in the layer followed by pairing and self-organization into larger vortices. At

the final simulation time we see two large counter-rotating vortices. The dissipation rate for this solution was studied in [26] confirming the qualitatively correct behaviour.

The second example we consider is KH instability on two-dimensional torus $\Gamma = \mathbb{T}^2 = \{\mathbf{x} \in \Omega \mid r^2 = x_3^2 + (\sqrt{x_1^2 + x_2^2} - R)^2\}$, with $R = 1$ and $r = 0.5$. The coordinate system is (ρ, ϕ, θ) , with

$$\mathbf{x} = R \begin{pmatrix} \cos \phi \\ \sin \phi \\ 0 \end{pmatrix} + \rho \begin{pmatrix} \cos \phi \cos \theta \\ \sin \phi \cos \theta \\ \sin \theta \end{pmatrix},$$

where ρ -direction is normal to Γ , $\frac{\partial \mathbf{x}}{\partial \rho} \perp \Gamma$ for $\mathbf{x} \in \Gamma$. In the torus coordinates, the initial velocity field is given by the same formula (4.1) with $\xi = \psi/(2\pi)$, $\zeta = \theta/(2\pi)$, and $d(\zeta) := d(\mathbf{x}(\xi, \zeta)) = \sqrt{x^2 + y^2} - 0.5$, $\mathbf{x} = (x, y, z)$, so that $d(\zeta)$ vanishes on the inner ring of the torus.

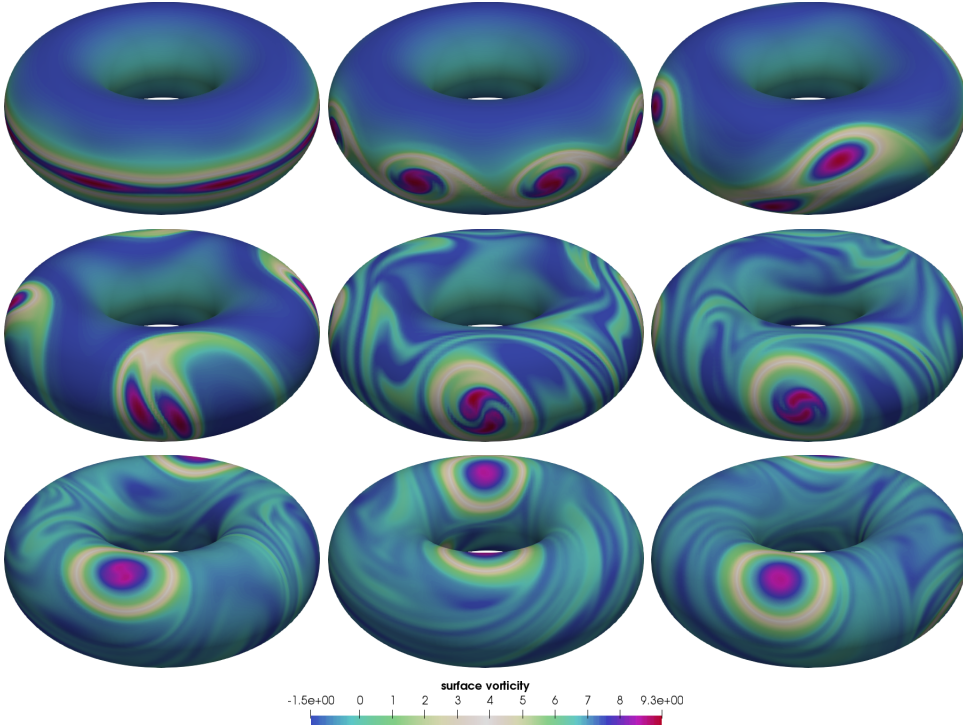


Fig. 4.2: Snapshots of surface vorticity $w_h = \text{curl}_{\Gamma_h} \mathbf{u}_h$ for KH on the $R = 1$, $r = \frac{1}{2}$ torus for $t \in \{0, 2.3, 8.4, 9.3, 14, 18.7, 25.7, 30.4, 35\}$. Click [here](#) for the full animation.

Figure 4.2 visualizes the vorticity field of the KH flow on the torus for $Re = 10^4$ ($\nu = \frac{1}{2} 10^{-5}$). The initial stage of the vortical layer formation and small vortices pairing is similar to the case of the sphere and the plane. The different geometry (and topology) of the torus apparently affects the interaction of larger vortices. From the time of about 20 units there are 4 large vortices formed, which further travel in the both toroidal and poloidal directions without pairing (see the animation): by the time of $t = 45$ we still observed the presence of 4 distinct vortices.

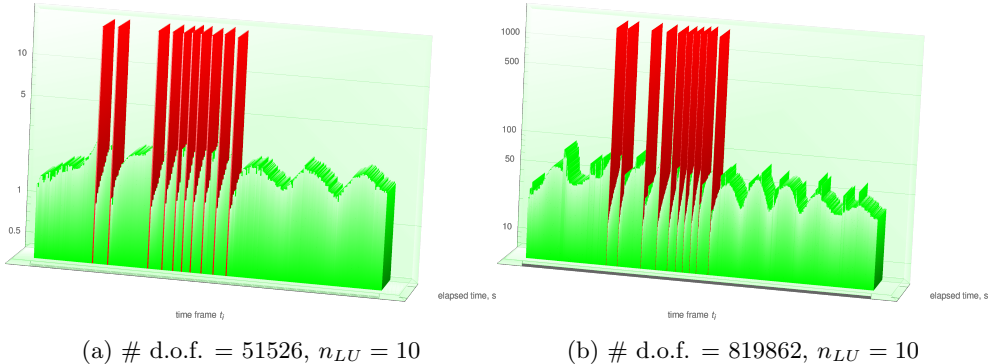


Fig. 4.3: Computation time seconds (factorization and linear solve) in log-scale vs. time t_i . Red bars correspond to time steps for which new factors are computed; n_{LU} is a number of steps with factorizations. Full AL preconditioner; Γ is the sphere.

Table 4.1: Solver statistics for $\nu = \frac{1}{2} \times 10^{-4}$, varying h and α . Full AL preconditioner; Γ is the sphere.

# d.o.f.	T_{asmb1}	% factor steps	“fresh” LU steps			all steps		
			N_{iter}	T_{factor}	T_{insol}	N_{iter}	T_{factor}	T_{insol}
51526	3.55	3.44	9.00	1.72×10^1	0.53	33.53	0.59	2.15
203998	18.6	1.88	8.33	1.76×10^2	2.55	32.77	3.30	10.3
819862	180	0.86	7.55	1.73×10^3	12.1	29.86	14.9	49.9

4.2. Solver performance. In the first series of experiments we fixed the viscosity parameter equal $\frac{1}{2}10^{-4}$ and vary the mesh size. We consider three levels of mesh refinement and the number of unknowns grows by a factor of four from one level to the next one. Since $\alpha \simeq 1/\Delta t$ and $\Delta t \simeq h$, the parameter α in (3.1) increases two times for each refinement level. The FGMRES with full AL preconditioner was applied to solve the system of algebraic equations on each time step of (2.3). We use zero vector as initial guess and the drop of residual by a factor of 10^8 as the stopping criterium. Table 4.1 summarizes the solver averaged statistics over the time of simulation $t \in [0, 20]$. We see that the percentage of re-initializations of the preconditioner (this is when we compute new LU factors) is small and decreases for finer mesh levels. The later can be due to the growth of α and because the the diffusion term plays more significant role for smaller h . The choice of $\kappa = 5$ in (3.7) keeps the average number of FGMRES iterations about 30 with very slight variation among refinement levels. To compare, the number of FGMRES iterations with ‘fresh’ LU factorization in $\hat{\mathbf{A}}$ is about 8. As expected, factorizing the matrix $\hat{\mathbf{A}}$ is by far the most computationally expensive procedure (cf. T_{factor} in “fresh LU steps” table section). However, due to the heavy and efficient recycling, overall the expense of the factorization is minor compared to the iterations cost (compare T_{factor} and T_{insol} in “all steps” table section). This allows to keep the *averaged* computation cost of the linear solver comparable

and even less than the cost of matrix assembling. This balance is further visualized in Figure 4.3 for two mesh levels, where we see that the time steps with updated LU factors are more expensive but rare. It is interesting to note that most updates are needed for $t \in [4, 10]$, when vortices are paring. As we discussed above, the numerical integration that we use causes the assembling time to grow superlinear with respect to #d.o.f.: This is the specific of the flow problem posed on a manifold and software we use for matrix assembly.

Table 4.2: Solver statistics for fixed h (# d.o.f. = 819862) and $\alpha \simeq 100$, varying ν . Full AL preconditioner; Γ is a sphere.

ν	$T_{\text{asmb}}l$	% factor steps	“fresh” LU steps			all steps		
			N_{iter}	T_{factor}	T_{linsol}	N_{iter}	T_{factor}	T_{linsol}
$\frac{1}{2} \times 10^{-3}$	177	0.391	7.00	1.59×10^3	9.87	32.87	6.23	50.7
$\frac{1}{2} \times 10^{-4}$	180	0.859	7.55	1.73×10^3	12.1	29.86	14.9	49.9
$\frac{1}{2} \times 10^{-5}$	198	0.938	7.75	1.81×10^3	12.4	31.95	17	50.2

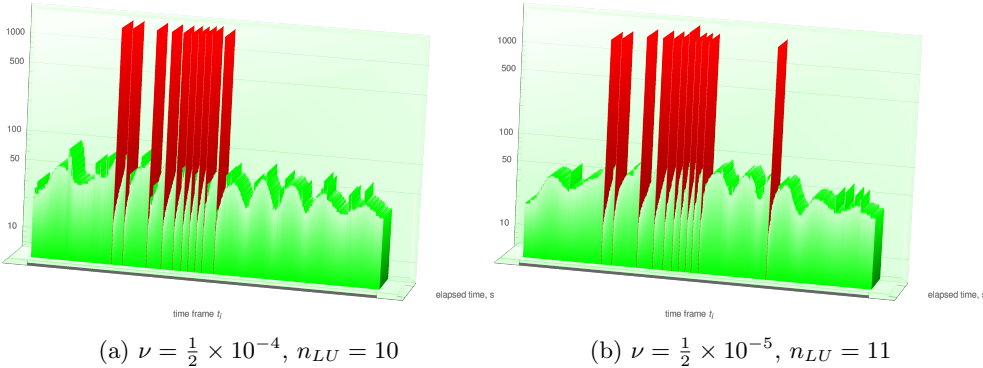


Fig. 4.4: Computation time seconds (matrix assembly and linear solve) in log-scale vs. time t_i . Red bars correspond to time steps for which factorization is performed; n_{LU} is a number of factorization steps. Full AL preconditioner; Γ is a sphere.

We repeat the simulation of the KH problem on the sphere but now for several values the viscosity parameter and the finest discretization level. All parameters of the algebraic solver are the same as above. The averaged statistics of the solver for this set of experiments are summarized in Table 4.2. It appears that the solver is remarkably robust with respect to the viscosity parameter. For higher Reynolds numbers we see only a slight increase of the percentage of time steps, where the preconditioner is updated by the new LU factors. Figure 4.4 illustrates the balance between computationally expensive but rare steps with updated preconditioner and the majority of calculations with the recycled AL preconditioner.

Table 4.3: Solver statistics for fixed $\nu = \frac{1}{2} \times 10^{-5}$, varying h and α . Modified AL preconditioner; Γ is a torus.

# d.o.f.	γ	T_{asmb1}	% factor steps	“fresh” LU steps			all steps		
				N_{iter}	T_{factor}	T_{linsol}	N_{iter}	T_{factor}	T_{linsol}
78244	0.028	7.65	6.25×10^{-1}	37.33	1.63	2.94	68.31	1.02×10^{-2}	5.02
315792	0.020	38.3	4.17×10^{-1}	42.75	18.1	16.3	75.32	7.55×10^{-2}	24.6
1279180	0.014	324	3.65×10^{-1}	64.71	181	97.6	75.51	6.61×10^{-1}	112

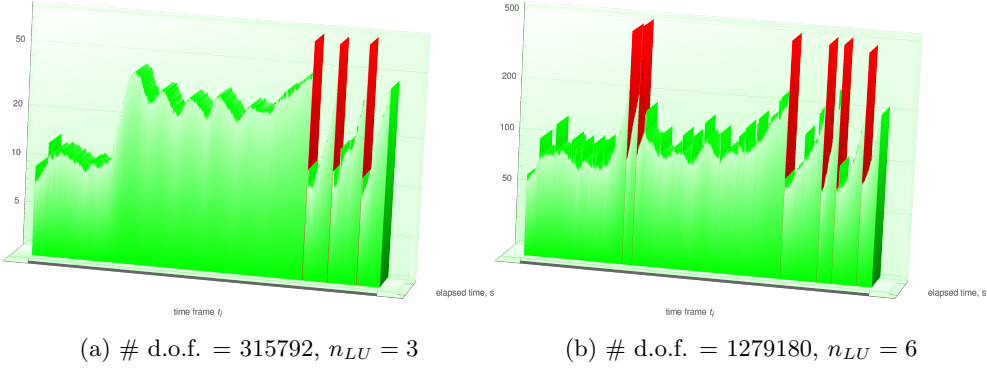


Fig. 4.5: Computation time seconds (matrix assembly and linear solve) in log-scale vs. time t_i . Red bars correspond to time steps for which new factors are computed; n_{LU} is a number of steps with factorizations. Modified AL preconditioner; Γ is a torus.

We now consider the surface KH flow on torus. For the given values of outer and inner radius the surface area of torus is approximately 1.57 times the surface of the unit sphere. This explains, why we get larger systems in terms of the number of degrees of freedom for the same levels of refinement in this example. This makes the problem naturally suitable for testing the recycling strategy with modified AL preconditioner. In general, the modified AL preconditioner is less robust with respect to ν and h , so its efficient use needs some tuning. Following recommendations in [3] we find optimal value for γ on a coarse level and then apply $1/\sqrt{2}$ -rule to scale it for finer mesh levels. This leads us to $\gamma_3 = 0.04$ for the third refinement level and $\gamma_i = 2^{\frac{3-i}{2}} \gamma_3$, $i = 4, 5, 6$, for refinement levels from 4 to 6. These are the refinement levels we use to report the solver statistics in Table 4.3. In this experiment, we take the velocity field and pressure from the previous time step as the initial guess in FGMRES and relax the stopping criterium to the relative drop of residual by 10^6 , $\|\mathbf{r}_i\|_2 < 10^{-6} \|\mathbf{b}\|_2$. The number of iterations increased compared to the full AL preconditioner, since only the block upper-triangle part of the matrix \mathbf{A} is used to define $\hat{\mathbf{A}}$. We also see a slight increase of the iteration number for h getting smaller, which is also the observation in [3]. The overall computation time is dominated by the matrix assembly because of the non-optimal numerical quadrature, as discussed above. If we take the time of assembly off the table, then the recycling strategy turns out to be very effective also

with the modified AL preconditioner. The average time of factorization per one solve is negligible and each factorization is more efficient in terms of time and memory requirements since it is done for each individual velocity block.

We expect that recycled modified AL preconditioner with a threshold ILU factorization for each sub-block can be an efficient strategy for large scale 3D flow problems, but we are not exploring such possibility here. We finally note that for multi-core architectures a lack of parallelism of the ILU factorization can be compensated by the high level of its reuse for the time-dependent flow problems within the suggested framework.

REFERENCES

- [1] M. BENZI, G. H. GOLUB, AND J. LIESEN, *Numerical solution of saddle point problems*, Acta numerica, 14 (2005), p. 1.
- [2] M. BENZI AND M. A. OLSHANSKII, *An augmented Lagrangian-based approach to the Oseen problem*, SIAM Journal on Scientific Computing, 28 (2006), pp. 2095–2113.
- [3] M. BENZI, M. A. OLSHANSKII, AND Z. WANG, *Modified augmented Lagrangian preconditioners for the incompressible Navier–Stokes equations*, International Journal for Numerical Methods in Fluids, 66 (2011), pp. 486–508.
- [4] A. BONITO, A. DEMLOW, AND M. LICHT, *A divergence-conforming finite element method for the surface stokes equation*, SIAM Journal on Numerical Analysis, 58 (2020), pp. 2764–2798.
- [5] S. BÖRM AND S. LE BORNE, *\mathcal{H} -LU factorization in preconditioners for augmented Lagrangian and grad-div stabilized saddle point systems*, International journal for numerical methods in fluids, 68 (2012), pp. 83–98.
- [6] P. BRANDNER AND A. REUSKEN, *Finite element error analysis of surface stokes equations in stream function formulation*, ESAIM: Mathematical Modelling and Numerical Analysis, 54 (2020), pp. 2069–2097.
- [7] E. BURMAN, P. HANSBO, AND M. G. LARSON, *A stabilized cut finite element method for partial differential equations on surfaces: The Laplace–Beltrami operator*, Computer Methods in Applied Mechanics and Engineering, 285 (2015), pp. 188–207.
- [8] E. BURMAN, P. HANSBO, M. G. LARSON, AND A. MASSING, *A cut discontinuous Galerkin method for the Laplace–Beltrami operator*, IMA Journal of Numerical Analysis, 37 (2017), pp. 138–169.
- [9] ———, *Cut finite element methods for partial differential equations on embedded manifolds of arbitrary codimensions*, ESAIM: Mathematical Modelling and Numerical Analysis, 52 (2018), pp. 2247–2282.
- [10] J. CAHOUEU AND J.-P. CHABARD, *Some fast 3D finite element solvers for the generalized Stokes problem*, International Journal for Numerical Methods in Fluids, 8 (1988), pp. 869–895.
- [11] O. DAHL AND S. WILLE, *An ILU preconditioner with coupled node fill-in for iterative solution of the mixed finite element formulation of the 2D and 3D Navier–Stokes equations*, International Journal for Numerical Methods in Fluids, 15 (1992), pp. 525–544.
- [12] A. DE NIET AND F. WUBS, *Two preconditioners for saddle point problems in fluid flows*, International Journal for Numerical Methods in Fluids, 54 (2007), pp. 355–377.
- [13] *DROPS package*. <http://www.igpm.rwth-aachen.de/DROPS/>.
- [14] H. ELMAN, D. SILVESTER, AND A. WATHEN, *Finite Elements and Fast Iterative Solvers*, Oxford University Press, Oxford, 2005.
- [15] P. E. FARRELL AND P. A. GAZCA-OROZCO, *An augmented Lagrangian preconditioner for implicitly-constituted non-Newtonian incompressible flow*, arXiv preprint arXiv:2005.03150, (2020).
- [16] P. E. FARRELL, L. MITCHELL, L. R. SCOTT, AND F. WECHSUNG, *A Reynolds-robust preconditioner for the Reynolds-robust Scott–Vogelius discretization of the stationary incompressible Navier–Stokes equations*, arXiv preprint arXiv:2004.09398, (2020).
- [17] P. E. FARRELL, L. MITCHELL, AND F. WECHSUNG, *An Augmented Lagrangian preconditioner for the 3D stationary incompressible Navier–Stokes equations at high Reynolds number*,

- SIAM Journal on Scientific Computing, 41 (2019), pp. A3073–A3096.
- [18] T.-P. FRIES, *Higher-order surface FEM for incompressible Navier–Stokes flows on manifolds*, International Journal for Numerical Methods in Fluids, 88 (2018), pp. 55–78.
 - [19] J. GRANDE, C. LEHRENFELD, AND A. REUSKEN, *Analysis of a high-order trace finite element method for PDEs on level set surfaces*, SIAM Journal on Numerical Analysis, 56 (2018), pp. 228–255.
 - [20] B. J. GROSS, N. TRASK, P. KUBERRY, AND P. J. ATZBERGER, *Meshfree methods on manifolds for hydrodynamic flows on curved surfaces: a generalized moving least-squares (GMLS) approach*, Journal of Computational Physics, 409 (2020), p. 109340.
 - [21] M. E. GURTIN AND A. I. MURDOCH, *A continuum theory of elastic material surfaces*, Archive for Rational Mechanics and Analysis, 57 (1975), pp. 291–323.
 - [22] X. HE, M. NEYTCHIEVA, AND S. S. CAPIZZANO, *On an augmented Lagrangian-based preconditioning of Oseen type problems*, BIT Numerical Mathematics, 51 (2011), pp. 865–888.
 - [23] X. HE, C. VUIK, AND C. M. KLAIJ, *Combining the augmented Lagrangian preconditioner with the simple Schur complement approximation*, SIAM Journal on Scientific Computing, 40 (2018), pp. A1362–A1385.
 - [24] T. HEISTER AND G. RAPIN, *Efficient augmented Lagrangian-type preconditioning for the Oseen problem using Grad-Div stabilization*, International Journal for Numerical Methods in Fluids, 71 (2013), pp. 118–134.
 - [25] T. JANKUHN, M. A. OLSHANSKII, AND A. REUSKEN, *Incompressible fluid problems on embedded surfaces: Modeling and variational formulations*, Interfaces and Free Boundaries, 20 (2018), pp. 353–377.
 - [26] T. JANKUHN, M. A. OLSHANSKII, A. REUSKEN, AND A. ZHILIAKOV, *Error analysis of higher order trace finite element methods for the surface Stokes equations*, Journal of Numerical Mathematics, (2020).
 - [27] T. JANKUHN AND A. REUSKEN, *Higher order trace finite element methods for the surface Stokes equation*, Preprint arXiv:1909.08327, (2019).
 - [28] V. JOHN AND A. KINDL, *Numerical studies of finite element variational multiscale methods for turbulent flow simulations*, Computer Methods in Applied Mechanics and Engineering, 199 (2010), pp. 841–852.
 - [29] I. KONSHIN, M. OLSHANSKII, AND Y. VASSILEVSKI, *LU factorizations and ILU preconditioning for stabilized discretizations of incompressible Navier–Stokes equations*, Numerical Linear Algebra with Applications, 24 (2017), p. e2085.
 - [30] I. N. KONSHIN, M. A. OLSHANSKII, AND Y. V. VASSILEVSKI, *ILU preconditioners for nonsymmetric saddle-point matrices with application to the incompressible Navier–Stokes equations*, SIAM Journal on Scientific Computing, 37 (2015), pp. A2171–A2197.
 - [31] P. L. LEDERER, C. LEHRENFELD, AND J. SCHÖBERL, *Divergence-free tangential finite element methods for incompressible flows on surfaces*, International Journal for Numerical Methods in Engineering, 121 (2020), pp. 2503–2533.
 - [32] C. LEHRENFELD, *High order unfitted finite element methods on level set domains using isoparametric mappings*, Computer Methods in Applied Mechanics and Engineering, 300 (2016), pp. 716–733.
 - [33] J. MOULIN, P. JOLIVET, AND O. MARQUET, *Augmented Lagrangian preconditioner for large-scale hydrodynamic stability analysis*, Computer Methods in Applied Mechanics and Engineering, 351 (2019), pp. 718–743.
 - [34] I. NITSCHKE, S. REUTHER, AND A. VOIGT, *Hydrodynamic interactions in polar liquid crystals on evolving surfaces*, Physical Review Fluids, 4 (2019), p. 044002.
 - [35] I. NITSCHKE, A. VOIGT, AND J. WENSCH, *A finite element approach to incompressible two-phase flow on manifolds*, Journal of Fluid Mechanics, 708 (2012), pp. 418–438.
 - [36] M. OLSHANSKII, G. LUBE, T. HEISTER, AND J. LÖWE, *Grad-div stabilization and subgrid pressure models for the incompressible Navier–Stokes equations*, Computer Methods in Applied Mechanics and Engineering, 198 (2009), pp. 3975–3988.
 - [37] M. OLSHANSKII AND A. REUSKEN, *Grad-div stabilization for Stokes equations*, Mathematics of Computation, 73 (2004), pp. 1699–1718.
 - [38] M. OLSHANSKII, A. REUSKEN, AND J. GRANDE, *A finite element method for elliptic equations on surfaces*, SIAM J. Numer. Anal., 47 (2009), pp. 3339–3358.

- [39] M. A. OLSHANSKII, *A low order Galerkin finite element method for the Navier–Stokes equations of steady incompressible flow: a stabilization issue and iterative methods*, Computer Methods in Applied Mechanics and Engineering, 191 (2002), pp. 5515–5536.
- [40] M. A. OLSHANSKII AND M. BENZI, *An augmented Lagrangian approach to linearized problems in hydrodynamic stability*, SIAM Journal on Scientific Computing, 30 (2008), pp. 1459–1473.
- [41] M. A. OLSHANSKII, A. QUAINI, A. REUSKEN, AND V. YUSHUTIN, *A finite element method for the surface Stokes problem*, SIAM Journal on Scientific Computing, 40 (2018), pp. A2492–A2518.
- [42] M. A. OLSHANSKII AND A. REUSKEN, *Trace finite element methods for PDEs on surfaces*, in Geometrically Unfitted Finite Element Methods and Applications, S. P. A. Bordas, E. Burman, M. G. Larson, and M. A. Olshanskii, eds., Cham, 2017, Springer International Publishing, pp. 211–258.
- [43] M. A. OLSHANSKII, A. REUSKEN, AND A. ZHILIAKOV, *Inf-sup stability of the trace P2-P1 Taylor–Hood elements for surface PDEs*, Mathematics of Computation, (2020).
- [44] M. A. OLSHANSKII AND V. YUSHUTIN, *A penalty finite element method for a fluid system posed on embedded surface*, Journal of Mathematical Fluid Mechanics, 21 (2019), p. 14.
- [45] P. RANGAMANI, A. AGRAWAL, K. K. MANDADAPU, G. OSTER, AND D. J. STEIGMANN, *Interaction between surface shape and intra-surface viscous flow on lipid membranes*, Biomechanics and modeling in mechanobiology, (2013), pp. 1–13.
- [46] S. REUTHER AND A. VOIGT, *Solving the incompressible surface Navier–Stokes equation by surface finite elements*, Physics of Fluids, 30 (2018), p. 012107.
- [47] P. W. SCHROEDER, V. JOHN, P. L. LEDERER, C. LEHRENFELD, G. LUBE, AND J. SCHÖBERL, *On reference solutions and the sensitivity of the 2D Kelvin–Helmholtz instability problem*, Computers & Mathematics with Applications, 77 (2019), pp. 1010–1028.
- [48] A. SEGAL, M. UR REHMAN, AND C. VUIK, *Preconditioners for incompressible Navier–Stokes solvers*, Numerical Mathematics: Theory, Methods and Applications, 3 (2010), pp. 245–275.
- [49] A. TORRES-SÁNCHEZ, D. MILLÁN, AND M. ARROYO, *Modelling fluid deformable surfaces with an emphasis on biological interfaces*, Journal of Fluid Mechanics, 872 (2019), pp. 218–271.
- [50] T. TRILINOS PROJECT TEAM, *The Trilinos Project Website*.
- [51] M. UR REHMAN, C. VUIK, AND G. SEGAL, *A comparison of preconditioners for incompressible Navier–Stokes solvers*, International Journal for Numerical methods in fluids, 57 (2008), pp. 1731–1751.